

# Scale-Invariant Models of Natural Oscillations in Chain Systems and Their Cosmological Significance

Hartmut Müller

E-mail: hm@interscalar.com

In this paper we review scale-invariant models of natural oscillations in chain systems of harmonic quantum oscillators and derive measurable consequences. Basic model claims are verified in terms of fundamental particles, the cosmic microwave background and the solar system. The cosmological significance of some model statements is discussed.

## Introduction

In the last 40 years many studies [1] were published which show that scale invariance (scaling) is a widely distributed phenomenon discovered in high energy physics [2–4], seismology [5, 6], biology [7–9] and stochastic processes of various nature [10].

As a property of power laws, scale invariance can be generated by very different mechanisms. The origin of power law relations and efforts to observe and validate them is a topic of research in many fields of science. However, the universality of scaling may have a mathematical origin that does not depend on the actual mechanism of manifestation.

In [11] we have shown that scale invariance is a fundamental property of natural oscillations in chain systems of similar harmonic oscillators. In [12] we applied this model on chain systems of harmonic quantum oscillators. In the case of a chain of protons as fundamental oscillators, particle rest masses coincide with the eigenstates of the system. This is valid not only for hadrons, but for mesons and leptons as well. Because of scale invariance, chains of electrons produce similar sets of natural frequencies.

In [13] Andreas Ries has shown that the complete description of elementary particle masses by the model of oscillations in chain systems is only possible if considering both, chains of protons and electrons. Furthermore, in [14] he was able to show that this model allows the prediction of the most abundant isotope for a given chemical element.

The core claims of scale-invariant models do not depend on the selection of the fundamental oscillator. Therefore, the rest mass of the fundamental oscillator can be even smaller than the electron mass. Consequently, all elementary particles can be interpreted as eigenstates in a chain system of harmonic quantum oscillators, in which the rest mass of each single oscillator goes to zero. This is how the transition of massless to massive states can be explained [15].

In [16] we have shown that scale-invariant models of natural oscillations in chain systems of protons also describe the mass distribution of large celestial bodies in the solar system.

The intention of this article is an adjustment of the basic claims of our model and an additional verification on fundamental particles, the cosmic microwave background and the

solar system. Furthermore, we discuss the cosmological significance of some model claims.

## 1 Methods

Kyryl Dombrowski [17] mentioned that oscillating systems – having the peculiarity to change their own parameters because of interactions inside the systems – have a tendency to reach a stable state where the individual oscillator frequencies are interrelated by specific numbers – namely minima of the rational number density on the number line.

Viktor and Maria Panchelyuga [18] showed that resonance phenomena appear more easily if they belong to maxima in the distribution of rational numbers, while maxima in the distribution of irrational numbers correspond with a high stability of the system, minimal interaction between parts of the system and minimal interaction with the surroundings.

In [11] we have shown that in the case of harmonic oscillations in chain systems, the set of natural frequencies is isomorphic to a discrete set of natural logarithms whose values are rational numbers.

Each real number (rational or irrational) has a biunique representation as a simple continued fraction. In addition, any rational number can be represented as a finite continued fraction and any finite continued fraction represents a rational number [19].

Consequently, the set of natural frequencies of a chain system of harmonic oscillators corresponds with a set of finite continued fractions  $\mathcal{F}$ , which are natural logarithms:

$$\begin{aligned} \ln(\omega_{jk}/\omega_{00}) &= n_{j0} + \frac{z}{n_{j1} + \frac{z}{n_{j2} + \dots + \frac{z}{n_{jk}}}} = \\ &= [z, n_{j0}; n_{j1}, n_{j2}, \dots, n_{jk}] = \mathcal{F}, \end{aligned} \quad (1)$$

where  $\omega_{jk}$  is the set of angular frequencies and  $\omega_{00}$  is the fundamental frequency of the set. The denominators are integer numbers:  $n_{j0}, n_{j1}, n_{j2}, \dots, n_{jk} \in \mathbb{Z}$ , the cardinality  $j \in \mathbb{N}$  of the set and the number  $k \in \mathbb{N}$  of layers are finite. In the canonical form, the numerator  $z$  is equal 1.

However, by means of the Euler equivalent transformation [20] every continued fraction with partial numerators

$z \neq 1$  can be changed into a continued fraction in the canonical form with  $z = 1$ .

Therefore, we will call the set  $\mathcal{F}$  of finite continued fractions (1) with  $z = 1$  the ‘‘Fundamental Fractal’’ of natural frequencies in chain systems of harmonic oscillators.

For rational exponents the natural exponential function is transcendental [21]. Therefore,  $\mathcal{F}$  is a set of transcendental numbers that is isomorphic to the set of rational numbers represented by finite continued fractions. The function of isomorphism is the natural logarithm.

It seems that this transcendence and consequently the irrationality of  $\mathcal{F}$  provides the high stability of the oscillating chain system because it avoids resonance interaction between the elements of the system.

### 2 Projections of the Fundamental Fractal

All elements of the continued fractions  $\mathcal{F}$  are integers and can therefore be represented as unique products of prime factors. Consequently, we can distinguish classes of finite continued fractions (classes of rational numbers) in dependency on the divisibility of the numerators and denominators by prime numbers, as we have shown in [11]. Based on this, different projections of  $\mathcal{F}$  can be studied.

Figure 1 demonstrates the formation of the canonical projection ( $z = 1$ ). Each vertical line represents a rational number that is the logarithm of a natural frequency of a chain system of harmonic oscillators.

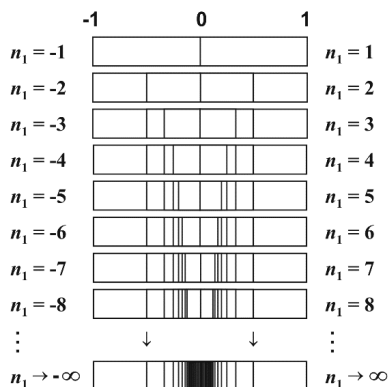


Fig. 1: The formation of the canonical projection ( $z = 1$ ) of the  $\mathcal{F}$  on the first layer  $k = 1$  (natural logarithmic representation).

The distribution density increases hyperbolically with  $|n_{j1}|$ . In the range  $1 < |n_{j1}| < 2$  the distribution density is minimum. Figure 2 shows that for finite continued fractions (1), ranges of high distribution density (nodes) arise near reciprocal integers  $1, 1/2, 1/3, 1/4, \dots$  which are the attractor points of the distribution.

All the denominators of the continued fractions  $\mathcal{F}$  are (positive and negative) integers. Therefore, the canonical projection is logarithmically symmetric, as figures 3 and 4 show.



Fig. 2: The canonical projection of the  $\mathcal{F}$  in the range  $0 \leq |n_{j0}| \leq 1$  for  $k = 2$  (natural logarithmic representation).

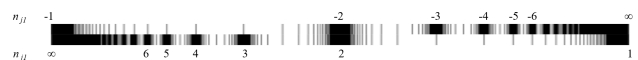


Fig. 3: The canonical projection of the  $\mathcal{F}$  in the range  $1 \leq |n_{j1}| < \infty$  for  $k = 2$  (natural logarithmic representation).

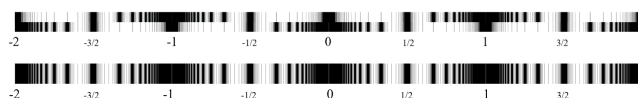


Fig. 4: The canonical projection of the  $\mathcal{F}$  in the range  $-2 \leq S \leq 2$  for  $k = 2$  (natural logarithmic representation).

In the following we investigate continued fractions (1) which meet the Markov [22] convergence condition  $|n| \geq |z| + 1$ .

Figure 5 illustrates different projections generated by continued fractions (1) with denominators divisible by 2, 3, 4, ... and the corresponding numerators  $z = 1, 2, 3, \dots$

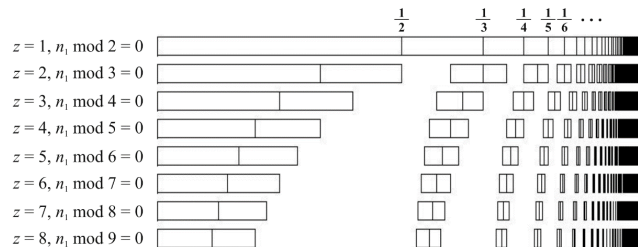


Fig. 5: Different projections generated by continued fractions (1) with denominators divisible by 2, 3, 4, ... and corresponding numerators  $z = 1, 2, 3, \dots$

Figure 5 shows the nodes on the first layer  $j = 1$  and also the borders of the node ranges, so the gaps are clearly visible. The borders of the gaps are determined by the alternating continued fractions  $[z, 0; z + 1, -z - 1, z + 1, -z - 1, \dots] = 1$  and  $[z, 0; z - 1, -z + 1, z - 1, -z + 1, \dots] = -1$ , for  $z \geq 1$ .

Denominators that are divisible by 3 with  $z = 2$  build the class of continued fractions (1) that generates the projection with the smallest gaps. These gaps remain empty even if the number of layers  $k$  increases infinitely.

In the  $2/3$ -projection, free links  $n_{j0}$  of the continued fractions (1) that are divisible by 3 designate the main nodes, denominators divisible by 3 designate subnodes while all the other denominators designate the borders of gaps (see Figure 6 and 7).

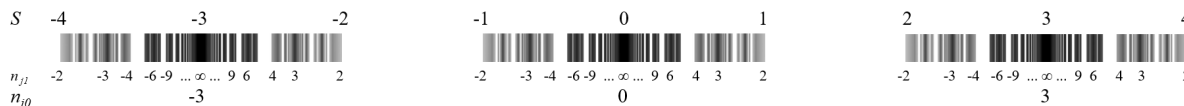


Fig. 6: The 2/3-projection of (1) with  $z = 2$ , divisible by 3  $|n_{j0}| = 3l$ , ( $l = 0, 1, 2, \dots$ ) and denominators divisible by 3  $|n_{jk}| = 3d$ , ( $d = 1, 2, \dots$ ) in the range of  $-4 \leq \mathcal{F} \leq 4$ .

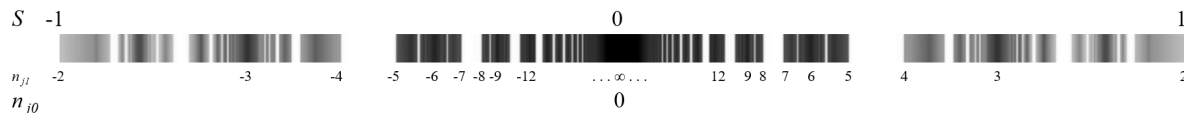


Fig. 7: The same 2/3-projection like in fig. 6, but in the range of  $-1 \leq \mathcal{F} \leq 1$ .

In [23] we have shown that in the 2/3-projection, ranges of gaps are connected with stochastic properties of natural oscillations in chain systems of protons. In the current paper we apply the canonical projection only.

### 3 Harmonic Scaling

Based on (1), we can now calculate the complete set  $\omega_{jk}$  of natural angular frequencies of a chain system of similar harmonic oscillators, if the fundamental frequency  $\omega_{00}$  or any other natural frequency of the set  $\omega_{jk}$  is known:

$$\omega_{jk} = \omega_{00} \exp(\mathcal{F}). \tag{2}$$

Here and in the following,  $\mathcal{F}$  is considered in its canonical projection with  $z = 1$ . The natural angular oscillation period  $\tau$  is defined as the reciprocal of the angular frequency:

$$\tau_{jk} = 1/\omega_{jk}. \tag{3}$$

The complete set of natural angular scale oscillation periods:

$$\tau_{jk} = \tau_{00} \exp(\mathcal{F}). \tag{4}$$

In [12] we have shown that our model (1) can be applied also in the case of natural oscillations in chain systems of harmonic quantum oscillators where the oscillation energy  $E$  depends only on the frequency ( $\hbar$  being the Planck constant):

$$E_{jk} = \hbar\omega_{jk}. \tag{5}$$

Consequently, the natural frequency set and the corresponding set of natural energies are isomorphic, so that chain systems of harmonic quantum oscillators generate discrete exponential energy series:

$$E_{jk} = E_{00} \exp(\mathcal{F}), \tag{6}$$

where  $E_{00} = \hbar\omega_{00}$  is the fundamental energy. Because of the mass-energy equivalence,

$$m_{jk} = E_{jk}/c^2 \tag{7}$$

the set of natural energies and the corresponding set of natural masses are isomorphic, so that chain systems of harmonic

quantum oscillators generate discrete exponential series of masses:

$$m_{jk} = m_{00} \exp(\mathcal{F}), \tag{8}$$

where  $m_{00} = \omega_{00} \cdot \hbar/c^2$  is the fundamental mass.

Finally, the set of natural frequencies corresponds to an isomorphic set of natural wavelengths ( $c$  being the speed of light in vacuum),

$$\lambda_{jk} = c/\omega_{jk} \tag{9}$$

so that chain systems of harmonic quantum oscillators generate discrete exponential series of natural wavelengths:

$$\lambda_{jk} = \lambda_{00} \exp(\mathcal{F}), \tag{10}$$

where  $\lambda_{00} = c/\omega_{00}$  is the fundamental wavelength.

As a consequence of (3) and (9), the set of natural wavelengths and the set of natural oscillation periods in chain systems of harmonic quantum oscillators coincide with an isomorphic set of natural velocities:

$$v_{jk} = \lambda_{jk}/\tau_{jk}. \tag{11}$$

Therefore, chain systems of harmonic quantum oscillators generate discrete exponential series of natural velocities as well:

$$v_{jk} = v_{00} \exp(\mathcal{F}), \tag{12}$$

where the fundamental velocity  $v_{00} = c$  is the speed of light in a vacuum.

In relation to the anticipated harmonic exponential series of wavelengths, velocities, energies and masses as a consequence of harmonic oscillations in chain systems, we propose the term ‘‘harmonic scaling’’.

The natural exponential function of a real argument  $x$  is the unique nontrivial function that is its own derivative

$$\frac{d}{dx} e^x = e^x$$

and therefore its own anti-derivative as well. Because of the self-similarity of the natural exponential function regarding its derivatives, any real number, being the result of a measurement, can be thought of as a natural logarithm or as the logarithm of a logarithm. Therefore, harmonic scaling is not

limited to exponentiation, but can be extended to tetration, pentation and other hyperoperations as well. In this case we will use the term “hyperscaling”.

#### 4 Harmonic Scaling of Fundamental Particles

In [12] we have shown that physical properties of fundamental particles, for example the proton-to-electron mass ratio or the vector boson-to-electron mass ratio, can be derived from eigenstates in chain systems of harmonic quantum oscillators.

In fact, the natural logarithm of the proton/neutron to electron mass ratio is close to  $[7; 2]$  and the logarithm of the W/Z-boson to proton mass ratio is near  $[4; 2]$ , so we can assume the equation:

$$\ln(m_{wz}/m_{pn}) = \ln(m_{pn}/m_e) - 3.$$

Consequently, the logarithm of the W/Z-boson to electron mass ratio is  $4\frac{1}{2} + 7\frac{1}{2} = 12$ :

$$\ln(m_{wz}/m_e) = 12,$$

where  $m_e$ ,  $m_{pn}$ ,  $m_{wz}$ , are the electron, proton/neutron and W/Z-boson rest masses. As table 1 shows, fundamental particle rest mass ratios correspond to attractor nodes of  $\mathcal{F}$ . Here and in the following we consider the continued fractions (1) in the canonical form, with the numerator  $z = 1$  and write them in square brackets.

Table 1: Fundamental particle rest masses and the corresponding attractor nodes of  $\mathcal{F}$ , with the electron mass as fundamental. Data taken from Particle Data Group.

particle	particle rest mass $m$ , MeV/ $c^2$	$\mathcal{F}$	$\ln(m/m_e)$	$\ln(m/m_e) - \mathcal{F}$
H-boson	$125090 \pm 240$	$[12; 2]$	12.408	-0.092
Z-boson	$91187.6 \pm 2.1$	$[12; \infty]$	12.092	0.092
W-boson	$80385 \pm 15$	$[12; \infty]$	11.966	-0.034
neutron	$939.565379 \pm 0.000021$	$[7; 2]$	7.517	0.017
proton	$938.272046 \pm 0.000021$	$[7; 2]$	7.515	0.015
electron	$0.510998928 \pm 0.000000011$	$[0; \infty]$	0.000	0.000

As table 1 shows, the logarithms of fundamental particle mass ratios are close to integer or half values that are rational numbers with the smallest possible numerators and denominators.

However, the natural logarithm of the W/Z-boson to proton mass ratio is not exactly 4.5, but between  $11.966 - 7.515 = 4.451$  and  $12.092 - 7.515 = 4.577$  that approximates  $\exp(3/2) = 4.4817$ . Thus, the properties of fundamental particle masses (table 1) also support our model of hyperscaling.

#### 5 Fundamental Metrology and Planck Units

The electron and the proton are exceptionally stable and therefore accessible anywhere in the universe. Their lifespan tops everything that is measurable, exceeding  $10^{29}$  years for

protons and  $10^{28}$  years for electrons [24]. In the framework of the standard theory of particle physics, the electron is stable because it is the least massive particle with non-zero electric charge. Its decay would violate charge conservation [25]. The proton is stable, because it is the lightest baryon and the baryon number is conserved as well. Therefore, the proton-to-electron mass ratio can be understood as a fundamental physical constant.

These unique properties of electrons and protons predetermine their physical characteristics as fundamental units. Table 2 shows the basic set of electron and proton units that can be considered as a fundamental metrology ( $c$  is the speed of light in a vacuum,  $\hbar$  is the Planck constant,  $k_B$  is the Boltzmann constant).

Table 2: The basic set of physical properties of the electron and proton. Data taken from Particle Data Group. Frequencies, oscillation periods, temperatures and the proton wavelength are calculated.

property	electron	proton
mass $m$	$9.10938356(11) \cdot 10^{-31}$ kg	$1.672621898(21) \cdot 10^{-27}$ kg
energy $E = mc^2$	$0.5109989461(31)$ MeV	$938.2720813(58)$ MeV
angular frequency $\omega = E/\hbar$	$7.76344071 \cdot 10^{20}$ Hz	$1.42548624 \cdot 10^{24}$ Hz
oscillation period $\tau = 1/\omega$	$1.28808867 \cdot 10^{-21}$ s	$7.01515 \cdot 10^{-25}$ s
wavelength $\lambda = c/\omega$	$3.8615926764(18) \cdot 10^{-13}$ m	$2.1030891 \cdot 10^{-16}$ m
temperature $T = mc^2/k_B$	$5.9298 \cdot 10^9$ K	$1.08881 \cdot 10^{13}$ m

In [15] we have shown that the Planck scale corresponds to a main attractor node of  $\mathcal{F}$  and consequently, Planck units [26] are completely compatible with the fundamental metrology (tab. 2).

Originally proposed in 1899 by Max Planck, these units are also known as natural units, because the origin of their definition comes only from properties of nature and not from any human construct.

Max Planck wrote [27] that these units, “regardless of any particular bodies or substances, retain their importance for all times and for all cultures, including alien and non-human, and can therefore be called natural units of measurement”. Planck units are based only on the properties of space-time.

In fact, the logarithm of the Planck-to-proton mass ratio is near the node  $[44; \infty]$  of the  $\mathcal{F}$ :

$$\ln\left(\frac{m_{\text{Planck}}}{m_{\text{proton}}}\right) = \ln\left(\frac{2.17647 \cdot 10^{-8}}{1.6726219 \cdot 10^{-27}}\right) = 44.012. \quad (13)$$

This fact does not only support our model (1), but allows us to derive the proton rest mass from the fundamental physical constants  $c$ ,  $\hbar$ ,  $G$ :

$$m_{\text{proton}} = \exp(-44)(\hbar c/G)^{1/2}. \quad (14)$$

In 1899, Max Planck noted that with his discovery of the quantum of action, sufficient fundamental constants were now

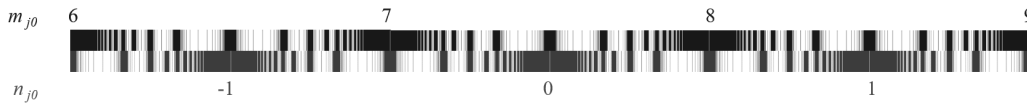


Fig. 8: The correspondence between electron-calibrated attractor nodes  $[m_{j0}]$  and proton-calibrated attractor nodes  $[n_{j0}]$  of  $\mathcal{F}$  in its canonical projection.

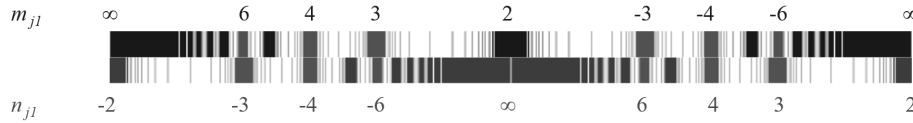


Fig. 9: The correspondence of electron-calibrated subnodes  $[m_{j0}; m_{j1}]$  to proton-calibrated subnodes  $[n_{j0}; n_{j1}]$  on the first layer of  $\mathcal{F}$  in the canonical projection.



Fig. 10: The correspondence of the electron-calibrated  $\mathcal{F}$  (above) to the proton-calibrated  $\mathcal{F}$  (below) in the  $2/3$ -projection.

known to define universal units for length, time, mass, and temperature.

This equation (14) may well be of cosmological significance, because it means that the values of proton and the electron rest masses are equally fundamental properties of space-time as are the speed of light, the Planck constant and the gravitational constant.

### 6 Cosmic Microwave Background

CMB data is critical to cosmology since any proposed model of the universe must explain this radiation. Within our model, the CMB can be understood as an eigenstate in a chain system of oscillating protons, because the black body temperature of the CMB corresponds to the main attractor node  $[-29; \infty]$  of the  $\mathcal{F}$  calibrated on the proton temperature (table 2):

$$\ln\left(\frac{T_{\text{CMB}}}{T_{\text{proton}}}\right) = \ln\left(\frac{2.726 \text{ K}}{1.08881 \cdot 10^{13} \text{ K}}\right) = -29.016. \quad (15)$$

### 7 Global Scaling

We hypothesise that harmonic scaling is a global phenomenon and continues in all scales, following the fundamental fractal (1) that is calibrated by this fundamental metrology (table 2). This hypothesis we have called ‘Global Scaling’ [23].

### 8 Calibration of the Fundamental Fractal

Table 1 shows that the natural logarithm of the proton-to-electron mass ratio is approximately 7.5 and consequently, the  $\mathcal{F}$  calibrated on the proton will be shifted by 7.5 logarithmic units relative to the  $\mathcal{F}$  calibrated on the electron. Figure 8 demonstrates this situation in the canonical projection.

As a consequence, all integer logarithms ( $n_{j1} = \infty$ ) of the proton  $\mathcal{F}$  correspond to half logarithms ( $m_{j1} = \pm 2$ ) of the electron  $\mathcal{F}$  and vice versa. In addition, the Diophantine equation (18) describes the correspondence of proton-calibrated subnodes  $[n_{j0}; n_{j1}]$  with electron-calibrated subnodes  $[m_{j0}; m_{j1}]$  on the first layer  $k = 1$  of  $\mathcal{F}$ :

$$\frac{1}{n_{j1}} + \frac{1}{m_{j1}} = \frac{1}{2}. \quad (16)$$

Only three pairs  $(n_{j1}, m_{j1})$  of integers are solutions to this equation: (4, 4), (3, 6) and (6, 3). Figure 9 demonstrates this correspondence.

In fact, if a process property corresponds to a half logarithm ( $m_{j1} = \pm 2$ ) of the electron calibrated  $\mathcal{F}$  it also corresponds to an integer logarithm ( $n_{j1} = \infty$ ) of the proton calibrated  $\mathcal{F}$ . Consequently, we must treat half logarithms and integer logarithms with equal (highest) priority. Furthermore, subnodes that satisfy the equation (16) are of high significance because the subnodes  $m_{j1} = \pm 3$ ,  $m_{j1} = \pm 4$  and  $m_{j1} = \pm 6$  of the electron  $\mathcal{F}$  coincide with the subnodes  $n_{j1} = \pm 6$ ,  $n_{j1} = \pm 4$  and  $n_{j1} = \pm 3$  of the proton  $\mathcal{F}$ . It is likely that this correspondence amplifies the attractor effect of these subnodes.

As figure 10 shows, in the  $2/3$ -projection, the electron-based  $\mathcal{F}$  (above) fills the empty intervals  $3l + 1 \leq S \leq 3l + 2$  ( $l = 0, 1, 2, \dots$ ) in the proton-based  $\mathcal{F}$  (below). Furthermore, in the intervals  $3l + 1/2 \leq S \leq 3l + 1$  ( $l = 0, 1, 2, \dots$ ) the proton  $\mathcal{F}$  overlaps with the electron  $\mathcal{F}$ . In the  $2/3$ -projection, the subnodes  $[2, n_{j0}; 3, -6]$  and  $[2, n_{j0}; -3, 6]$  in the logarithmic center of the overlapping area are the only nodes that are common to both the proton-based and electron-based  $\mathcal{F}$ .

In [23] we have applied the  $2/3$ -projection on the Solar system. In the following, we will test our hypothesis of global scaling on the Solar system applying the canonical projection.

## 9 Applying Global Scaling on the Solar System

In 2010 we have shown [16] that the masses of large celestial bodies in the Solar system continue the scale-invariant sequence of fundamental particle rest masses (see table 1), corresponding with main attractor nodes of the fundamental fractal (1).

If we consider the Solar system as still evolving – at least in terms of small body collisions and matter exchanges with neighbouring systems – the expected attractor effect of nodes suggests applying  $\mathcal{F}$  for the prediction of evolutionary trends.

Yet, the existence of stable orbits and large celestial bodies with stable rotation periods suggests testing our hypothesis of global scaling on the Solar system. Let us begin with the most noticeable examples.

### The Sun

The current amount of the Solar mass supports our hypothesis of global scaling, because it corresponds to a main attractor node of the electron-calibrated  $\mathcal{F}$  (8). In fact, the natural logarithm of the Sun-to-electron mass ratio is close to an integer number:

$$\ln\left(\frac{M_{\text{Sun}}}{m_{\text{electron}}}\right) = \ln\left(\frac{1.9884 \cdot 10^{30} \text{ kg}}{9.10938356 \cdot 10^{-31} \text{ kg}}\right) = 138.936.$$

Also, the Solar radius corresponds to a main attractor node of the electron  $\mathcal{F}$  (10):

$$\ln\left(\frac{R_{\text{Sun}}}{\lambda_{\text{electron}}}\right) = \ln\left(\frac{6.96407 \cdot 10^8 \text{ m}}{3.8615926764 \cdot 10^{-13} \text{ m}}\right) = 48.945.$$

The Solar sidereal rotation period is in between  $\tau_{\text{min}} = 24.5$  days at the equator and  $\tau_{\text{max}} = 34.4$  days at the poles. The canonical projection of the electron  $\mathcal{F}$  (4) shows that the Solar rotation period varies between the main attractor node [63;  $\infty$ ] and its nearest significant subnode [63; -3]:

$$\ln\left(\frac{\tau_{\text{max}}}{\tau_{\text{electron}}}\right) = \ln\left(\frac{34.4 \cdot 86164 \text{ s}}{1.28808867 \cdot 10^{-21} \text{ s}}\right) = 63.003,$$

$$\ln\left(\frac{\tau_{\text{min}}}{\tau_{\text{electron}}}\right) = \ln\left(\frac{24.5 \cdot 86164 \text{ s}}{1.28808867 \cdot 10^{-21} \text{ s}}\right) = 62.664.$$

### Jupiter

Let's start with Jupiter's body mass:

$$\ln\left(\frac{M_{\text{Jupiter}}}{m_{\text{electron}}}\right) = \ln\left(\frac{1.8986 \cdot 10^{27} \text{ kg}}{9.10938356 \cdot 10^{-31} \text{ kg}}\right) = 131.981$$

we can see that the Jupiter body mass corresponds to the main attractor node [132;  $\infty$ ] of the electron  $\mathcal{F}$  (8) and within our model, the body mass of Jupiter  $M_{\text{Jupiter}}$  can be calculated from the Solar Mass  $M_{\text{Sun}}$ , by simply dividing it seven times by the Euler number  $e = 2.71828 \dots$ :

$$M_{\text{Jupiter}} = \frac{M_{\text{Sun}}}{\exp(7)}. \quad (17)$$

Jupiter's body radius corresponds to the significant subnode [47; -3] of the electron  $\mathcal{F}$  (10):

$$\ln\left(\frac{R_{\text{Jupiter}}}{\lambda_{\text{electron}}}\right) = \ln\left(\frac{7.1492 \cdot 10^7 \text{ m}}{3.8615926764 \cdot 10^{-13} \text{ m}}\right) = 46.668.$$

The sidereal rotation period of Jupiter is 9.925 hours and corresponds with the main attractor node [66;  $\infty$ ] of the proton  $\mathcal{F}$  (4):

$$\ln\left(\frac{\tau_{\text{Jupiter}}}{\tau_{\text{proton}}}\right) = \ln\left(\frac{9.925 \cdot 3600 \text{ s}}{7.01515 \cdot 10^{-25} \text{ s}}\right) = 66.100.$$

In contrast to rotation as angular movement, the location of a celestial body in the Solar system in orbital movement changes permanently. Furthermore, in the case of non-zero eccentricity, the angular velocity of orbital movement is not constant. Therefore, we expect that the orbital periods coincide with attractor nodes of the  $\mathcal{F}$  (4) with the electron oscillation period  $2\pi\tau_e$  as the fundamental. For example, Jupiter's orbital period of 4332.59 days fulfils the conditions of global scaling very precisely:

$$\ln\left(\frac{T_{\text{Jupiter}}}{2\pi\tau_{\text{electron}}}\right) = \ln\left(\frac{4332.59 \cdot 86164 \text{ s}}{8.0932998 \cdot 10^{-21} \text{ s}}\right) = 66.001.$$

When the logarithm of the sidereal rotation period of Jupiter slows down to [66;  $\infty$ ], the orbital-to-rotation period ratio of Jupiter can be described by the equation:

$$\frac{T_{\text{Jupiter}}}{\tau_{\text{Jupiter}}} = 2\pi \frac{\tau_{\text{electron}}}{\tau_{\text{proton}}}. \quad (18)$$

The orbital velocity of Jupiter is between  $v_{\text{min}} = 12.44$  and  $v_{\text{max}} = 13.72$  km/s. This velocity clearly approximates the main attractor node [-10;  $\infty$ ] of the  $\mathcal{F}$  calibrated on the speed of light (12):

$$\ln\left(\frac{v_{\text{max}}}{c}\right) = \ln\left(\frac{13720 \text{ m/s}}{299792458 \text{ m/s}}\right) = -9.992,$$

$$\ln\left(\frac{v_{\text{min}}}{c}\right) = \ln\left(\frac{12440 \text{ m/s}}{299792458 \text{ m/s}}\right) = -10.090.$$

Consequently, the orbital distance of Jupiter between Perihelion = 4.95029 and Aphelion = 5.45492 astronomical units approximates the main attractor node [56;  $\infty$ ] of the electron-calibrated  $\mathcal{F}$  (10):

$$\ln\left(\frac{A_{\text{Jupiter}}}{\lambda_{\text{electron}}}\right) = \ln\left(\frac{5.45492 \cdot 149597870700 \text{ m}}{3.8615926764 \cdot 10^{-13} \text{ m}}\right) = 56.011,$$

$$\ln\left(\frac{P_{\text{Jupiter}}}{\lambda_{\text{electron}}}\right) = \ln\left(\frac{4.95029 \cdot 149597870700 \text{ m}}{3.8615926764 \cdot 10^{-13} \text{ m}}\right) = 55.914.$$

By the way, the masses of Jupiter's largest moons fulfil the condition of global scaling as well. For example, the body

mass of Ganymede fits perfectly with the main node [115;  $\infty$ ] of the proton  $\mathcal{F}$  (8):

$$\ln\left(\frac{M_{\text{Ganymede}}}{m_{\text{proton}}}\right) = \ln\left(\frac{1.4819 \cdot 10^{23} \text{ kg}}{1.672621 \cdot 10^{-27} \text{ kg}}\right) = 115.009.$$

On the other hand, the body mass of Io corresponds with the significant subnode [114; 2]:

$$\ln\left(\frac{M_{\text{Io}}}{m_{\text{proton}}}\right) = \ln\left(\frac{8.9319 \cdot 10^{22} \text{ kg}}{1.672621 \cdot 10^{-27} \text{ kg}}\right) = 114.502.$$

### Venus

The morning star is another impressive example of global scaling. Like the Sun or Jupiter, the body mass of Venus corresponds to a main attractor node of the electron  $\mathcal{F}$  (8):

$$\ln\left(\frac{M_{\text{Venus}}}{m_{\text{electron}}}\right) = \ln\left(\frac{4.8675 \cdot 10^{24} \text{ kg}}{9.10938356 \cdot 10^{-31} \text{ kg}}\right) = 126.015.$$

Although the rotation of Venus is reverse, its rotation period of 5816.66728 hours fits perfectly with the main attractor node [65;  $\infty$ ] of the electron calibrated  $\mathcal{F}$  (4):

$$\ln\left(\frac{\tau_{\text{Venus}}}{\tau_{\text{electron}}}\right) = \ln\left(\frac{5816.66728 \cdot 3600 \text{ s}}{1.28808867 \cdot 10^{-21} \text{ s}}\right) = 64.958.$$

The sidereal orbital period of Venus of 224.701 days fulfils the condition of global scaling as well:

$$\ln\left(\frac{T_{\text{Venus}}}{2\pi\tau_{\text{electron}}}\right) = \ln\left(\frac{224.701 \cdot 86164 \text{ s}}{2\pi \cdot 1.28808867 \cdot 10^{-21} \text{ s}}\right) = 63.042.$$

The orbital velocity of Venus ( $v_{\text{min}} = 34.79$  and  $v_{\text{max}} = 35.26$  km/s) corresponds well to the main attractor node [-9;  $\infty$ ] of the speed of light calibrated  $\mathcal{F}$  (12):

$$\ln\left(\frac{v_{\text{max}}}{c}\right) = \ln\left(\frac{35260 \text{ m/s}}{299792458 \text{ m/s}}\right) = -9.048,$$

$$\ln\left(\frac{v_{\text{min}}}{c}\right) = \ln\left(\frac{34790 \text{ m/s}}{299792458 \text{ m/s}}\right) = -9.062.$$

The orbital distance of Venus (Perihelion=0.71844 and Aphelion = 0.728213 astronomical units) corresponds precisely to the main attractor node [54;  $\infty$ ] of the electron calibrated  $\mathcal{F}$  (10):

$$\ln\left(\frac{A_{\text{Venus}}}{\lambda_{\text{electron}}}\right) = \ln\left(\frac{0.728213 \cdot 149597870700 \text{ m}}{3.8615926764 \cdot 10^{-13} \text{ m}}\right) = 53.997,$$

$$\ln\left(\frac{P_{\text{Venus}}}{\lambda_{\text{electron}}}\right) = \ln\left(\frac{0.718440 \cdot 149597870700 \text{ m}}{3.8615926764 \cdot 10^{-13} \text{ m}}\right) = 53.984.$$

The current body radius of Venus corresponds with the subnode [44; 5] of the electron  $\mathcal{F}$  (10):

$$\ln\left(\frac{R_{\text{Venus}}}{\lambda_{\text{electron}}}\right) = \ln\left(\frac{6.053 \cdot 10^6 \text{ m}}{3.8615926764 \cdot 10^{-13} \text{ m}}\right) = 44.199.$$

However, its vicinity to the significant subnode [44; 4] gives reason to expect that Venus is still growing.

### Mars

Again, the body mass of Mars corresponds to a main attractor node of the electron  $\mathcal{F}$  (8):

$$\ln\left(\frac{M_{\text{Mars}}}{m_{\text{electron}}}\right) = \ln\left(\frac{6.4171 \cdot 10^{23} \text{ kg}}{9.10938356 \cdot 10^{-31} \text{ kg}}\right) = 123.989.$$

The sidereal rotation period of Mars is 24.62278 hours and coincides perfectly to the main node [67;  $\infty$ ] of the proton  $\mathcal{F}$  (4):

$$\ln\left(\frac{\tau_{\text{Mars}}}{\tau_{\text{proton}}}\right) = \ln\left(\frac{24.62278 \cdot 3600 \text{ s}}{7.01515 \cdot 10^{-25} \text{ s}}\right) = 67.008.$$

The orbital velocity of Mars is between 21.97 and 26.50 km/s, approximating the subnode [-9; -2] of the speed of light calibrated  $\mathcal{F}$  (12):

$$\ln\left(\frac{v_{\text{max}}}{c}\right) = \ln\left(\frac{26500 \text{ m/s}}{299792458 \text{ m/s}}\right) = -9.334,$$

$$\ln\left(\frac{v_{\text{min}}}{c}\right) = \ln\left(\frac{21970 \text{ m/s}}{299792458 \text{ m/s}}\right) = -9.521.$$

In addition, the orbital period of Mars 686.971 days meets precisely the condition of global scaling:

$$\ln\left(\frac{T_{\text{Mars}}}{2\pi\tau_{\text{electron}}}\right) = \ln\left(\frac{686.971 \cdot 86164 \text{ s}}{2\pi \cdot 1.28808867 \cdot 10^{-21} \text{ s}}\right) = 65.997.$$

The orbital distance of Mars (Perihelion = 1.3814 and Aphelion = 1.6660 astronomical units) approximates the significant subnode [55; -4] of the electron  $\mathcal{F}$  (10):

$$\ln\left(\frac{A_{\text{Mars}}}{\lambda_{\text{electron}}}\right) = \ln\left(\frac{1.6660 \cdot 149597870700 \text{ m}}{3.8615926764 \cdot 10^{-13} \text{ m}}\right) = 54.825,$$

$$\ln\left(\frac{P_{\text{Mars}}}{\lambda_{\text{electron}}}\right) = \ln\left(\frac{1.3814 \cdot 149597870700 \text{ m}}{3.8615926764 \cdot 10^{-13} \text{ m}}\right) = 54.637.$$

The current body radius of Mars is close to the significant subnode [44; -3] of the  $\mathcal{F}$  (10):

$$\ln\left(\frac{R_{\text{Mars}}}{\lambda_{\text{electron}}}\right) = \ln\left(\frac{3.396 \cdot 10^6 \text{ m}}{3.8615926764 \cdot 10^{-13} \text{ m}}\right) = 43.621.$$

It is therefore likely that Mars, too, is still growing. From this point of view, the large Martian canyon (Valles Marineris) can be interpreted as a sign of crustal swelling [28].

### Earth

The current mass of the Earth corresponds to the significant subnode [126; 4] of the electron  $\mathcal{F}$  (8):

$$\ln\left(\frac{M_{\text{Earth}}}{m_{\text{electron}}}\right) = \ln\left(\frac{5.97237 \cdot 10^{24} \text{ kg}}{9.10938356 \cdot 10^{-31} \text{ kg}}\right) = 126.220.$$

Hence, we can expect that the Earth is slightly increasing its mass.

The body radius of the Earth approximates precisely the significant subnode [44; 4] of the electron  $\mathcal{F}$  (10):

$$\ln\left(\frac{R_{\text{Earth equator}}}{\lambda_{\text{electron}}}\right) = \ln\left(\frac{6.378 \cdot 10^3 \text{ m}}{3.8615926764 \cdot 10^{-13} \text{ m}}\right) = 44.251,$$

$$\ln\left(\frac{R_{\text{Earth pole}}}{\lambda_{\text{electron}}}\right) = \ln\left(\frac{6.357 \cdot 10^3 \text{ m}}{3.8615926764 \cdot 10^{-13} \text{ m}}\right) = 44.248.$$

The sidereal rotation period of the Earth is 23.93444 hours and is located very close to the main node [67;  $\infty$ ] in the proton  $\mathcal{F}$  (4):

$$\ln\left(\frac{\tau_{\text{Earth}}}{\tau_{\text{proton}}}\right) = \ln\left(\frac{23.93444 \cdot 3600 \text{ s}}{7.01515 \cdot 10^{-25} \text{ s}}\right) = 66.980,$$

Therefore, we can expect that the rotation period of the Earth is also slightly increasing. Empirical studies [29] confirm the correlation between body mass and rotation period.

Earth's orbital period of 365.256363 days is close to the main attractor node [71] of the proton-based  $\mathcal{F}$  (4):

$$\ln\left(\frac{T_{\text{Earth}}}{2\pi\tau_{\text{proton}}}\right) = \ln\left(\frac{365.256363 \cdot 86164 \text{ s}}{2\pi \cdot 7.01515 \cdot 10^{-25} \text{ s}}\right) = 71.043.$$

Earth's orbital velocity is between  $v_{\min} = 29.29$  and  $v_{\max} = 30.29$  km/s, approximating the significant subnode [-9; 4] of the speed of light-based  $\mathcal{F}$  (12):

$$\ln\left(\frac{v_{\max}}{c}\right) = \ln\left(\frac{30290 \text{ m/s}}{299792458 \text{ m/s}}\right) = -9.200,$$

$$\ln\left(\frac{v_{\min}}{c}\right) = \ln\left(\frac{29290 \text{ m/s}}{299792458 \text{ m/s}}\right) = -9.234,$$

The orbital distance of the Earth (Perihelion = 0.9832687 and Aphelion = 1.01673 astronomical units) corresponds to the significant subnode [54; 3] of the electron-based  $\mathcal{F}$  (10):

$$\ln\left(\frac{A_{\text{Earth}}}{\lambda_{\text{electron}}}\right) = \ln\left(\frac{1.0167300 \cdot 149597870700 \text{ m}}{3.8615926764 \cdot 10^{-13} \text{ m}}\right) = 54.331,$$

$$\ln\left(\frac{P_{\text{Earth}}}{\lambda_{\text{electron}}}\right) = \ln\left(\frac{0.9832687 \cdot 149597870700 \text{ m}}{3.8615926764 \cdot 10^{-13} \text{ m}}\right) = 54.297.$$

### Mercury

Mercury's body mass is close to the significant subnode [123; 3] of the electron  $\mathcal{F}$  (8):

$$\ln\left(\frac{M_{\text{Mercury}}}{m_{\text{electron}}}\right) = \ln\left(\frac{3.3011 \cdot 10^{23} \text{ kg}}{9.10938356 \cdot 10^{-31} \text{ kg}}\right) = 123.324.$$

Its body radius is close to the significant subnode [43; 3] of the electron  $\mathcal{F}$  (10):

$$\ln\left(\frac{R_{\text{Mercury}}}{\lambda_{\text{electron}}}\right) = \ln\left(\frac{2.44 \cdot 10^3 \text{ m}}{3.8615926764 \cdot 10^{-13} \text{ m}}\right) = 43.290.$$

So we can expect that Mercury is slightly increasing its mass and size. The sidereal rotation period of Mercury is 1407.5 hours and corresponds to the main attractor node [71;  $\infty$ ] of the proton  $\mathcal{F}$  (4):

$$\ln\left(\frac{\tau_{\text{Mercury}}}{\tau_{\text{proton}}}\right) = \ln\left(\frac{1407.5 \cdot 3600 \text{ s}}{7.01515 \cdot 10^{-25} \text{ s}}\right) = 71.054.$$

The sidereal orbital period of Mercury of 87.9691 days is close to the main attractor node [62;  $\infty$ ] of the electron  $\mathcal{F}$  (4):

$$\ln\left(\frac{T_{\text{Mercury}}}{2\pi\tau_{\text{electron}}}\right) = \ln\left(\frac{87.9691 \cdot 86164 \text{ s}}{2\pi \cdot 1.28808867 \cdot 10^{-21} \text{ s}}\right) = 62.104.$$

The orbital velocity of Mercury oscillates between the main attractor node [-9;  $\infty$ ] and the significant subnode [-9; 2] of the speed of light calibrated  $\mathcal{F}$  (12):

$$\ln\left(\frac{v_{\max}}{c}\right) = \ln\left(\frac{58980 \text{ m/s}}{299792458 \text{ m/s}}\right) = -8.534,$$

$$\ln\left(\frac{v_{\min}}{c}\right) = \ln\left(\frac{38860 \text{ m/s}}{299792458 \text{ m/s}}\right) = -8.951.$$

Mercury's Aphelion corresponds to the main attractor node [61;  $\infty$ ] of the proton calibrated  $\mathcal{F}$  (10):

$$\ln\left(\frac{A_{\text{Mercury}}}{\lambda_{\text{proton}}}\right) = \ln\left(\frac{0.466697 \cdot 149597870700 \text{ m}}{2.1030891 \cdot 10^{-16} \text{ m}}\right) = 61.067.$$

### Saturn

Saturn's body mass is close to the significant subnode [131; -4] of the electron calibrated  $\mathcal{F}$  (8),

$$\ln\left(\frac{M_{\text{Saturn}}}{m_{\text{electron}}}\right) = \ln\left(\frac{5.6836 \cdot 10^{23} \text{ kg}}{9.10938356 \cdot 10^{-31} \text{ kg}}\right) = 130.776$$

so we suspect that Saturn is actually losing mass and that its ring system is part of the loss process.

The sidereal rotation period of Saturn is 10.55 hours and corresponds to the significant subnode [59; -3] of the electron  $\mathcal{F}$  (4):

$$\ln\left(\frac{\tau_{\text{Saturn}}}{\tau_{\text{electron}}}\right) = \ln\left(\frac{10.55 \cdot 3600 \text{ s}}{1.28808867 \cdot 10^{-21} \text{ s}}\right) = 58.646.$$

Therefore, we may expect that Saturn is slightly slowing down its rotation. The orbital period of Saturn of 10759.22 days corresponds to the main attractor node [67;  $\infty$ ] of the electron  $\mathcal{F}$  (4):

$$\ln\left(\frac{T_{\text{Saturn}}}{2\pi\tau_{\text{electron}}}\right) = \ln\left(\frac{10759.22 \cdot 86164 \text{ s}}{2\pi \cdot 1.28808867 \cdot 10^{-21} \text{ s}}\right) = 66.911.$$

Therefore, we may predict that Saturn is slightly increasing its orbit.

The current orbital velocity of Saturn is between 9.09 and 10.18 km/s, approximating the significant subnode  $[-10; 3]$  of the speed of light calibrated  $\mathcal{F}$  (12):

$$\ln\left(\frac{v_{\max}}{c}\right) = \ln\left(\frac{10180 \text{ m/s}}{299792458 \text{ m/s}}\right) = -10.290,$$

$$\ln\left(\frac{v_{\min}}{c}\right) = \ln\left(\frac{9090 \text{ m/s}}{299792458 \text{ m/s}}\right) = -10.404.$$

The orbital distance of Saturn is between Perihelion = 9.024 and Aphelion = 10.086 astronomical units, oscillating between the significant subnodes  $[57; -2]$  and  $[57; -3]$  of the electron  $\mathcal{F}$  (10):

$$\ln\left(\frac{A_{\text{Saturn}}}{\lambda_{\text{electron}}}\right) = \ln\left(\frac{10.086 \cdot 149597870700 \text{ m}}{3.8615926764 \cdot 10^{-13} \text{ m}}\right) = 56.625,$$

$$\ln\left(\frac{P_{\text{Saturn}}}{\lambda_{\text{electron}}}\right) = \ln\left(\frac{9.024 \cdot 149597870700 \text{ m}}{3.8615926764 \cdot 10^{-13} \text{ m}}\right) = 56.514.$$

Saturn's equatorial body radius is very close to the significant subnode  $[46; 2]$  of the electron  $\mathcal{F}$  (10):

$$\ln\left(\frac{R_{\text{Saturn}}}{\lambda_{\text{electron}}}\right) = \ln\left(\frac{6.0268 \cdot 10^7 \text{ m}}{3.8615926764 \cdot 10^{-13} \text{ m}}\right) = 46.497$$

and consequently, to the main attractor node  $[54; \infty]$  of the proton  $\mathcal{F}$  (10) as well:

$$\ln\left(\frac{R_{\text{Saturn}}}{\lambda_{\text{proton}}}\right) = \ln\left(\frac{6.0268 \cdot 10^7 \text{ m}}{2.1030891 \cdot 10^{-16} \text{ m}}\right) = 54.012.$$

Furthermore, Titan's body mass is near the main node  $[115; \infty]$  of the proton  $\mathcal{F}$  (8):

$$\ln\left(\frac{M_{\text{Titan}}}{m_{\text{proton}}}\right) = \ln\left(\frac{1.3452 \cdot 10^{23} \text{ kg}}{1.672621 \cdot 10^{-27} \text{ kg}}\right) = 114.912.$$

## Uranus

To reach the nearby main attractor node  $[129; \infty]$  of the electron-based  $\mathcal{F}$  (8), Uranus must increase its body mass by approx. 1/10 logarithmic units:

$$\ln\left(\frac{M_{\text{Uranus}}}{m_{\text{electron}}}\right) = \ln\left(\frac{8.681 \cdot 10^{25} \text{ kg}}{9.10938356 \cdot 10^{-31} \text{ kg}}\right) = 128.897.$$

The orbital period of Uranus of 30688.5 days corresponds to the main attractor node  $[68; \infty]$  of the electron-based  $\mathcal{F}$  (4):

$$\ln\left(\frac{T_{\text{Uranus}}}{2\pi\tau_{\text{electron}}}\right) = \ln\left(\frac{30688.5 \cdot 86164 \text{ s}}{2\pi \cdot 1.28808867 \cdot 10^{-21} \text{ s}}\right) = 67.959,$$

Like Neptune, the body radius of Uranus is close to the significant subnode  $[46; -3]$  of the electron  $\mathcal{F}$  (10):

$$\ln\left(\frac{R_{\text{Uranus}}}{\lambda_{\text{electron}}}\right) = \ln\left(\frac{2.5559 \cdot 10^7 \text{ m}}{3.8615926764 \cdot 10^{-13} \text{ m}}\right) = 45.639.$$

We may therefore expect that Uranus, like Neptune, is slightly swelling.

The orbital distance of Uranus (Perihelion = 18.33 and Aphelion = 20.11 astronomical units) approximates the significant subnode  $[57; 4]$  of the electron  $\mathcal{F}$  (10):

$$\ln\left(\frac{A_{\text{Uranus}}}{\lambda_{\text{electron}}}\right) = \ln\left(\frac{20.11 \cdot 149597870700 \text{ m}}{3.8615926764 \cdot 10^{-13} \text{ m}}\right) = 57.315,$$

$$\ln\left(\frac{P_{\text{Uranus}}}{\lambda_{\text{electron}}}\right) = \ln\left(\frac{18.33 \cdot 149597870700 \text{ m}}{3.8615926764 \cdot 10^{-13} \text{ m}}\right) = 57.223.$$

The orbital velocity of Uranus is between 6.49 and 7.11 km/s, approximating the significant subnode  $[-11; 3]$  of the speed of light calibrated  $\mathcal{F}$  (12):

$$\ln\left(\frac{v_{\max}}{c}\right) = \ln\left(\frac{7110 \text{ m/s}}{299792458 \text{ m/s}}\right) = -10.741,$$

$$\ln\left(\frac{v_{\min}}{c}\right) = \ln\left(\frac{6490 \text{ m/s}}{299792458 \text{ m/s}}\right) = -10.649.$$

The sidereal rotation period of Uranus is 17.24 hours and corresponds to the significant subnode  $[67; -3]$  of the proton  $\mathcal{F}$  (4):

$$\ln\left(\frac{\tau_{\text{Uranus}}}{\tau_{\text{proton}}}\right) = \ln\left(\frac{17.24 \cdot 3600 \text{ s}}{7.01515 \cdot 10^{-25} \text{ s}}\right) = 66.652.$$

Therefore, we can expect that Uranus is slightly slowing down its rotation.

## Neptune

Neptune's body mass corresponds to the main attractor node  $[129; \infty]$  of the electron calibrated  $\mathcal{F}$  (8):

$$\ln\left(\frac{M_{\text{Neptune}}}{m_{\text{electron}}}\right) = \ln\left(\frac{1.0243 \cdot 10^{26} \text{ kg}}{9.10938356 \cdot 10^{-31} \text{ kg}}\right) = 129.062.$$

The sidereal rotation period of Neptune is 16.11 hours and coincides perfectly with the main attractor node  $[59; \infty]$  of the electron-calibrated  $\mathcal{F}$  (4):

$$\ln\left(\frac{\tau_{\text{Neptune}}}{\tau_{\text{electron}}}\right) = \ln\left(\frac{16.11 \cdot 3600 \text{ s}}{1.28808867 \cdot 10^{-21} \text{ s}}\right) = 59.069.$$

The orbital velocity of Neptune is between 5.37 and 5.50 km/s, close to the main node  $[-11; \infty]$  of the speed of light calibrated  $\mathcal{F}$  (12):

$$\ln\left(\frac{v_{\max}}{c}\right) = \ln\left(\frac{5500 \text{ m/s}}{299792458 \text{ m/s}}\right) = -10.930,$$

$$\ln\left(\frac{v_{\min}}{c}\right) = \ln\left(\frac{5370 \text{ m/s}}{299792458 \text{ m/s}}\right) = -10.906.$$

Neptune's current orbital distance (Perihelion = 29.81 and Aphelion = 30.33 astronomical units) corresponds to the significant subnode [58; -4] of the electron-calibrated  $\mathcal{F}$  (10):

$$\ln\left(\frac{A_{\text{Neptune}}}{\lambda_{\text{electron}}}\right) = \ln\left(\frac{30.33 \cdot 149597870700 \text{ m}}{3.8615926764 \cdot 10^{-13} \text{ m}}\right) = 57.726,$$

$$\ln\left(\frac{P_{\text{Neptune}}}{\lambda_{\text{electron}}}\right) = \ln\left(\frac{29.81 \cdot 149597870700 \text{ m}}{3.8615926764 \cdot 10^{-13} \text{ m}}\right) = 57.709.$$

Because of the assumed attractor effect of the main node [-11;  $\infty$ ] of the  $\mathcal{F}$  (12), we can expect that the logarithm of Neptune's orbital velocity should decrease by nearly 1/10. At the same time, the logarithm of Neptune's orbital distance should increase by almost 1/20 due to the attractor effect of the significant subnode [58; -4] of the  $\mathcal{F}$  (10). This trend forecast agrees with the Kepler laws: for circular Solar orbits, the orbital velocity of a planet changes with the square root of its orbital distance.

In addition, Neptune's orbital period of 60182 days is close to the significant subnode [69; -3] of the electron  $\mathcal{F}$  (4):

$$\ln\left(\frac{T_{\text{Neptune}}}{2\pi\tau_{\text{electron}}}\right) = \ln\left(\frac{60182 \cdot 86164 \text{ s}}{2\pi \cdot 1.28808867 \cdot 10^{-21} \text{ s}}\right) = 68.632.$$

This value supports our trend estimation that Neptune's orbit is slightly growing.

The current body radius of Neptune is close to the significant subnode [46; -3] of  $\mathcal{F}$  (10):

$$\ln\left(\frac{R_{\text{Neptune}}}{\lambda_{\text{electron}}}\right) = \ln\left(\frac{2.4764 \cdot 10^7 \text{ m}}{3.8615926764 \cdot 10^{-13} \text{ m}}\right) = 45.607.$$

And so, we can expect that Neptune is still swelling.

### Pluto

Although Pluto is no longer considered a planet, its body mass corresponds well with the main attractor node [120;  $\infty$ ] of the electron  $\mathcal{F}$  (8):

$$\ln\left(\frac{M_{\text{Pluto}}}{m_{\text{electron}}}\right) = \ln\left(\frac{1.305 \cdot 10^{22} \text{ kg}}{9.10938356 \cdot 10^{-31} \text{ kg}}\right) = 120.094.$$

The orbital period of Pluto of 90560 days corresponds to the main attractor node [69;  $\infty$ ] of the electron  $\mathcal{F}$  (4):

$$\ln\left(\frac{T_{\text{Pluto}}}{2\pi\tau_{\text{electron}}}\right) = \ln\left(\frac{90560 \cdot 86164 \text{ s}}{2\pi \cdot 1.28808867 \cdot 10^{-21} \text{ s}}\right) = 69.044.$$

The sidereal rotation period of Pluto is 152.87496 hours and corresponds to the significant subnode [61; 3] of the electron-calibrated  $\mathcal{F}$  (4):

$$\ln\left(\frac{\tau_{\text{Pluto}}}{\tau_{\text{electron}}}\right) = \ln\left(\frac{152.87496 \cdot 3600 \text{ s}}{1.28808867 \cdot 10^{-21} \text{ s}}\right) = 61.319.$$

Therefore, we can expect that Pluto is slightly slowing down in its rotation.

The orbital velocity of Pluto oscillates between 3.71 and 6.10 km/s, approximating the main attractor node [-11;  $\infty$ ] of the speed of light calibrated  $\mathcal{F}$  (12):

$$\ln\left(\frac{v_{\text{max}}}{c}\right) = \ln\left(\frac{6100 \text{ m/s}}{299792458 \text{ m/s}}\right) = -10.803,$$

$$\ln\left(\frac{v_{\text{min}}}{c}\right) = \ln\left(\frac{3710 \text{ m/s}}{299792458 \text{ m/s}}\right) = -11.300.$$

The orbital distance of Pluto (Perihelion = 29.656 and Aphelion = 49.319 astronomical units) approximates the main attractor node [58;  $\infty$ ] of the electron-calibrated  $\mathcal{F}$  (10):

$$\ln\left(\frac{A_{\text{Pluto}}}{\lambda_{\text{electron}}}\right) = \ln\left(\frac{49.319 \cdot 149597870700 \text{ m}}{3.8615926764 \cdot 10^{-13} \text{ m}}\right) = 58.212,$$

$$\ln\left(\frac{P_{\text{Pluto}}}{\lambda_{\text{electron}}}\right) = \ln\left(\frac{29.656 \cdot 149597870700 \text{ m}}{3.8615926764 \cdot 10^{-13} \text{ m}}\right) = 57.704.$$

The body radius of Pluto  $1187 \pm 7$  km is close to the significant subnode [42; 2] of the electron-calibrated  $\mathcal{F}$  (10),

$$\ln\left(\frac{R_{\text{Pluto}}}{\lambda_{\text{electron}}}\right) = \ln\left(\frac{1187 \cdot 10^6 \text{ m}}{3.8615926764 \cdot 10^{-13} \text{ m}}\right) = 42.570,$$

which is also close to the main attractor node [50;  $\infty$ ] of the proton-calibrated  $\mathcal{F}$  (10):

$$\ln\left(\frac{R_{\text{Pluto}}}{\lambda_{\text{proton}}}\right) = \ln\left(\frac{1187 \cdot 10^6 \text{ m}}{2.1030891 \cdot 10^{-16} \text{ m}}\right) = 50.085.$$

Hence, we can expect that Pluto is slightly shrinking. This prognosis matches with new findings of surface-atmosphere interactions and mass wasting processes [30] on Pluto.

By the way, also Charon's body mass fits with the main node [118;  $\infty$ ] of the electron  $\mathcal{F}$  (8):

$$\ln\left(\frac{M_{\text{Charon}}}{m_{\text{electron}}}\right) = \ln\left(\frac{1.587 \cdot 10^{21} \text{ kg}}{9.10938356 \cdot 10^{-31} \text{ kg}}\right) = 117.944.$$

In conclusion, table 3 gives an overview of the current positions in the electron calibrated  $\mathcal{F}$  (4), (8), (10), and (12) of the Sun and the planets (including Pluto) regarding their masses, sizes, rotation, orbital distances, periods and velocities.

Table 3 shows that our model (1) allows to see a connection between the stability of the Solar system and the stability of electron and proton. Jupiter, Neptune, Venus and Pluto occupy mostly main attractor nodes of the electron calibrated fundamental fractal  $\mathcal{F}$  and therefore they can be understood as electron determined factors of stability in the Solar system. It is interesting that also the Sun occupies main nodes of the electron  $\mathcal{F}$ . Considering the coincidence of half logarithms in the electron  $\mathcal{F}$  with integer logarithms (main attractor nodes) of the proton  $\mathcal{F}$ , the stability of Earth's rotation and orbit seems connected with the stability of the proton. Furthermore, Earth's mass and radius occupy the subnode  $n_1 = 4$  that is maximum distant from any main attractor node of the  $\mathcal{F}$ . This position could be connected with some optimum of flexibility, if we consider the main nodes as islands of stability.

Table 3: The current positions in the electron calibrated  $\mathcal{F}(4)$ , (8), (10) and (12) of the largest bodies regarding their masses, sizes, rotation, orbital distances, periods and velocities. In the cases of large eccentricity\*, the logarithmically average position is indicated.

celestial body	mass in $\mathcal{F}(8)$	radius in $\mathcal{F}(10)$	rotation period in $\mathcal{F}(4)$	orbital period in $\mathcal{F}(4)$	orbital distance in $\mathcal{F}(10)$	orbital velocity in $\mathcal{F}(12)$
Sun	[139; $\infty$ ]	[49; $\infty$ ]	[63; $\infty$ ]			
Jupiter	[132; $\infty$ ]	[47; -3]	[58; 2]	[66; $\infty$ ]	[56; $\infty$ ]	[-10; $\infty$ ]
Saturn	[131; -4]	[46; 2]	[59; -3]	[67; $\infty$ ]	[56; 2]	[-10; -3]
Neptune	[129; $\infty$ ]	[46; -3]	[59; $\infty$ ]	[69; -3]	[58; -4]	[-11; $\infty$ ]
Uranus	[129; $\infty$ ]	[46; -3]	[59; 6]	[68; $\infty$ ]	[57; 4]	[-11; 3]
Earth	[126; 4]	[44; 4]	[59; 2]	[63; 2]	[54; 3]	[-9; -4]
Venus	[126; $\infty$ ]	[44; 4]	[65; $\infty$ ]	[63; $\infty$ ]	[54; $\infty$ ]	[-9; $\infty$ ]
Mars	[124; $\infty$ ]	[44; -3]	[59; 2]	[64; 6]	[55; -4]	[-9; -2]
Mercury	[123; 3]	[43; 3]	[63; 2]	[62; 6]	[53; 3]*	[-9; 3]*
Pluto	[120; $\infty$ ]	[42; 2]	[61; 3]	[69; $\infty$ ]	[58; $\infty$ ]*	[-11; $\infty$ ]*

**Resume**

Properties of fundamental particles, for example the proton-to-electron mass ratio or the vector boson-to-electron mass ratio (table 1), support our scale-invariant model (1) of eigenstates in chain systems of harmonic quantum oscillators and have allowed us to derive the proton rest mass from fundamental physical constants (14). In addition, the cosmic microwave background can be interpreted as an eigenstate of a chain system of oscillating protons (15).

In our scale-invariant model, physical properties of celestial bodies such as mass, size, rotation and orbital period can be understood as macroscopic quantized eigenstates of chain systems of oscillating protons and electrons. This understanding can be applied to evolutionary trend prognosis of the Solar system but may be of cosmological significance as well. Conceivably, the observable exponential expansion of the universe is a consequence of the scale-invariance of the fundamental fractal (1).

**Acknowledgements**

The author is grateful to Viktor Panchelyuga for valuable discussions and support.

Submitted on July 18, 2017

**References**

- Barenblatt G. I. Scaling. Cambridge University Press, 2003.
- Feynman R. P. Very High-Energy Collisions of Hadrons. *Phys. Rev. Lett.*, 1969, 23, 1415.
- Kolombet V. Macroscopic fluctuations, masses of particles and discrete space-time. *Biofizika*, 1992, v. 36, 492–499 (in Russian).
- Tatischeff B. Fractals and log-periodic corrections applied to masses and energy levels of several nuclei. arXiv:1107.1976v1 [physics.gen-ph] 11 Jul 2011.
- Gutenberg B., Richter C. F., Seismicity of the Earth and Associated Phenomena, 2nd ed. Princeton, N.J., Princeton University Press, 1954.
- Corral A. Universal local versus unified global scaling laws in the statistics of seismicity. arXiv:cond-mat/0402555 v1 23 Feb 2004.
- Čislenko L. L. The Structure of the Fauna and Flora in connection with the sizes of the organisms. Moscow, 1981 (in Russian).

- Schmidt-Nielsen K. Scaling. Why is the animal size so important? Cambridge University Press, 1984.
- Zhirmunsky A. V., Kuzmin V. I. Critical levels in developmental processes of biological systems. Moscow, Nauka, 1982 (in Russian).
- Shnoll S. E. Changes in the fine structure of stochastic distributions as a consequence of space-time fluctuations. arxiv.org/ftp/physics/papers/0602/0602017.
- Müller H. Fractal Scaling Models of Resonant Oscillations in Chain Systems of Harmonic Oscillators. *Progress in Physics*, 2009, issue 2, 72–76.
- Müller H. Fractal Scaling Models of Natural Oscillations in Chain Systems and the Mass Distribution of Particles. *Progress in Physics*, 2010, issue 3, 61–66.
- Ries A. Bipolar Model of Oscillations in a Chain System for Elementary Particle Masses. *Progress in Physics*, 2012, issue 4, 20–28.
- Ries A. Qualitative Prediction of Isotope Abundances with the Bipolar Model of Oscillations in a Chain System. *Progress in Physics*, 2015, issue 11, 183–186.
- Müller H. Emergence of Particle Masses in Fractal Scaling Models of Matter. *Progress in Physics*, 2012, issue 4, 44–47.
- Müller H. Fractal scaling models of natural oscillations in chain systems and the mass distribution of the celestial bodies in the Solar System. *Progress in Physics*, 2010, issue 3, 61–66.  
Müller H. Scaling of body masses and orbital periods in the Solar system as consequence of gravity interaction elasticity. Abstracts of the XII. International Conference on Gravitation, Astrophysics and Cosmology, dedicated to the centenary of Einstein’s General Relativity theory. Moscow, PFUR, 2015.
- Dombrowski K. I. Rational numbers distribution and resonance. *Progress in Physics*, 2005, v. 1, 65–67.
- Panchelyuga V. A., Panchelyuga M. S. Resonance and Fractals on the Real Numbers Set. *Progress in Physics*, 2012, issue 4, 48–53.
- Khinchine A. Ya. Continued fractions. University of Chicago Press, Chicago, 1964.
- Skorobogatko V. Ya. The Theory of Branched Continued Fractions and mathematical Applications. Moscow, Nauka, 1983.
- Hilbert D. Über die Transcendenz der Zahlen  $e$  und  $\pi$ . *Mathematische Annalen*, 1893, 43, 216–219.
- Markov A. A. Selected work on the continued fraction theory and theory of functions which are minimum divergent from zero. Moscow – Leningrad, 1948 (In Russian).
- Müller H. Scaling as Fundamental Property of Natural Oscillations and the Fractal Structure of Space-Time. Foundations of Physics and Geometry. Peoples Friendship University of Russia, 2008 (in Russian).
- Olive K. A. et al. (Particle Data Group), *Chin. Phys. C.*, 2016, v. 38, 090001.
- Steinberg R. I. et al. Experimental test of charge conservation and the stability of the electron. *Physical Review D*, 1999, 61 (2), 2582–2586.
- Astrophysical constants. Particle Data Group, pdg.lbl.gov
- Max Planck. Über Irreversible Strahlungsvorgänge. In: *Sitzungsbericht der Königlich Preußischen Akademie der Wissenschaften*, 1899, vol. 1, 479–480.
- Lin An. Structural analysis of the Valles Marineris fault zone: Possible evidence for large-scale strike-slip faulting on Mars. *Lithosphere*, 2012, 4 (4), 286–330.
- Gizachew Tiruneh. Explaining Planetary-Rotation Periods Using an Inductive Method. arXiv: 0906.3531 [astro-ph.SR]
- Stern S. A. et al. The Pluto system: Initial results from its exploration by New Horizons. *Science*, 2015, 350(6258), 249–352; arXiv:1510.07704.